Nondestructive Testing Using mm-Wave Sparse Imaging Verified for Singly Curved Composite Panels

Wingren, Niklas; Sjöberg, Daniel

Published in:
IEEE Transactions on Antennas and Propagation

DOI:
10.1109/TAP.2022.3211341

2022

Document Version:
Peer reviewed version (aka post-print)

Communication

Nondestructive Testing Using mm-Wave Sparse Imaging Verified for Singly Curved Composite Panels

Niklas Wingren and Daniel Sjöberg

***Abstract*—Nondestructive testing of composite materials is important in aerospace applications, and mm-wave imaging has been increasingly used for this purpose. Imaging is traditionally performed using Fourier methods, with inverse methods being an alternative. This communication presents a mm-wave imaging method with an inverse approach intended for nondestructive testing of singly curved composite panels with sparsely distributed flaws. It builds on previous work which was limited to imaging on planar panels. The move from planar to singly curved panels increases the applicability of the method for aerospace applications. The imaging method is reference-free due to a numerical source separation algorithm and exploits sparsity in reconstruction of scatterers. It is demonstrated using near-field measurements at 60 GHz of an industrially manufactured composite panel with deliberate flaws. Compared to a more traditional Fourier imaging method, our method generates images with higher resolution and higher dynamic range. Flaw detection is also easier using our method as it generates images with less background clutter.**

***Index Terms*—Image reconstruction, inverse problems, microwave imaging, nondestructive testing, source separation.**

I. Introduction

Composite materials are increasingly used for a wide range of applications such as automotive parts, sports equipment and aerospace structures [1]. Specifically in aerospace, reasons for using composite materials can be their high strength-to-weight ratio and electromagnetic (EM) performance [2]. The latter is especially important for radomes, but also for aircraft structural components in some cases. Doubly curved and singly curved structures are used for aerodynamic surfaces, with singly curved structures being less costly and easier to manufacture [3]. During production and maintenance of such structures, nondestructive testing (NDT) is typically performed to detect flaws without detrimental effects on performance [4]. An interesting method for NDT in general, and for evaluation of EM properties of composites in particular is millimeter wave (mm-wave) (30-300 GHz) imaging [5], [6]. One of its main advantages is an inherently high resolution, but there are many others such as contactless operation, compact systems and a relatively low cost [5], [7]. A typical mm-wave imaging system consists of a transmitting (Tx) antenna illuminating the DUT, and a receiving (Rx) antenna sampling the signal scattered by the DUT at a set of spatial points. This sampling can be done in a simple way by mechanically scanning a single Rx antenna between the desired spatial points [8].

A traditional way of performing microwave and mm-wave imaging is through Fourier methods. One common example is synthetic aperture radar (SAR), which has proven useful in a wide range of NDT applications [9]–[12]. SAR is traditionally performed by sampling the scattered signal over one spatial dimension and using a large bandwidth to obtain a two dimensional image [13]. A Fourier method with close similarities to SAR is time reversal imaging (commonly known as migration in geophysics) [14], [15]. In contrast to traditional SAR, this method can be performed using a single frequency but with sampling of the scattered signal over two spatial dimensions. If sampling is performed in a plane, the signal can be translated to other parallel planes, which allows for simple imaging on a planar DUT.

Imaging can also be approached as an inverse problem, often using methods from computational electromagnetics where the fundamental EM equations are solved numerically [16]–[20]. As with time reversal imaging, inverse methods can be performed with spatial sampling in a plane using a single frequency. However, while time reversal imaging results in images in parallel planes, the inverse approach allows for images conformal to an arbitrary DUT surface [21]. One way of setting up the imaging problem from fundamental EM equations is with an inverse equivalent source formulation, where the known signal is related to unknown currents using an integral equation. This integral equation is then discretized to obtain a linear system of equations which can be solved to obtain the currents [20]–[22]. The system is often not solved directly, but through the use of appropriate optimization methods. Methods utilizing L_1-minimization have shown promise for the solution of underdetermined systems where the solution is known beforehand to be sparse in the selected basis [23], [24].

This communication builds upon the previous work in [25] and [26] where an inverse equivalent source technique was developed to generate high resolution and high dynamic range mm-wave images of planar DUTs. A source separation technique was used to estimate the scattered signal without the need for a reference measurement, and an L_1-minimization technique was used for sparse scatterer reconstruction on the DUT. The sparsity in the reconstruction stemmed from the intended application of industrially manufactured low-loss, low-permittivity aerospace composite panels, as flaws were then assumed to be few and physically small.

This work was supported in part by the Swedish Armed Forces, in part by the Swedish Defence Materiel Administration, in part by the National Aeronautics Research Program and in part by the Swedish Governmental Agency for Innovation Systems. *(Corresponding author: Niklas Wingren.)*

The authors are with the Department of Electrical and Information Technology, Lund University, SE-221 00 Lund, Sweden (e-mail: niklas.wingren@eit.lth.se, daniel.sjoberg@eit.lth.se).

Color versions of one or more of the figures in this paper are available online at http://ieeexplore.ieee.org.

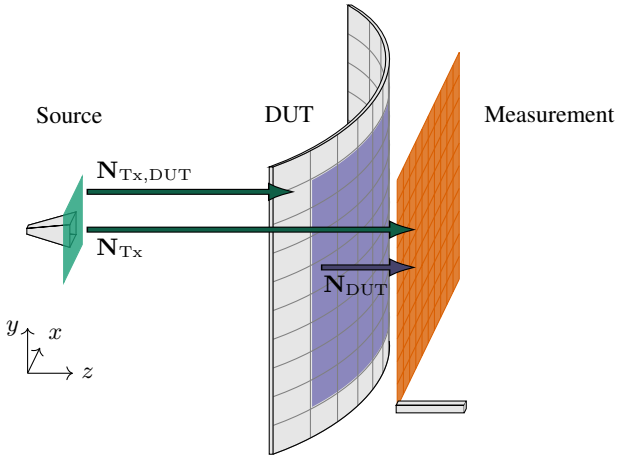

Fig. 1. Illustration of the measurement setup with surfaces of interest (source, DUT, measurement) highlighted and operators between surfaces as arrows.

The purpose of this communication is to demonstrate transmission-based imaging on a singly curved surface enclosing a DUT. If the DUT is itself singly curved, the image can be conformal to its surface. This makes the method more suited towards the intended application of NDT of aerospace structures as it extends the possible geometries of DUTs. As singly curved structures are less difficult and costly to manufacture than doubly curved structures, the extension of the DUT geometry made in this work is expected to be relevant for many realistic structures. The images presented in this communication use data from near-field measurements at 60 GHz of an industrially manufactured singly curved composite panel. For comparison, images are generated both using the inverse approach and more conventional time reversal imaging. As in previous work, the images produced using the sparse imaging approach have high resolution and high dynamic range, especially when compared to those produced using time reversal.

The communication is organized as follows. Section II briefly describes the imaging algorithms of interest. Section III describes the experimental setup used to retrieve data. Section IV presents and discusses imaging results, which is followed by conclusions in Section V.

II. Imaging Algorithms

The problem of interest is visualized in Fig. 1 where a source (the Tx antenna) illuminates a singly curved DUT and the transmitted signal is measured in a planar grid by the Rx antenna. The objective of an imaging algorithm is to use the data from the measurement plane to reconstruct an image of the DUT showing EM flaws. An inverse equivalent source approach is used to reconstruct equivalent electric currents on a planar surface in front of the source and a singly curved surface on the DUT (the surfaces highlighted in Fig. 1). For this purpose, operators mapping electrical currents to electric fields are used, with operators of interest drawn in Fig. 1. The details of this approach are found in [25], [26] for planar surfaces, and in this work we primarily highlight the differences required for imaging on singly curved surfaces.

The sparse imaging used in this work specifically uses two steps detailed in [25], [26]: source separation and L_1-minimization. The source separation step uses a truncated singular value decomposition (SVD) regularization to numerically estimate the field due to the source and the background medium of the DUT. This is then subtracted from the measured data, resulting in a field due to flaws in the DUT without use of a reference measurement. The general methodology is independent of DUT geometry, and as such it is the same as used in earlier work.

The L_1-minimization step is used to reconstruct flaws using the data from the source separation step. The nominal manufacturing quality is deemed to be good enough that flaws are few and far apart, which corresponds to a sparsity condition for scatterers in a pixel basis. Due to this, the imaging problem is formulated as a basis pursuit denoising problem [24], which reads

$$\hat{\boldsymbol{s}} = \arg\min_{\boldsymbol{s}} \|\boldsymbol{s}\|_1 \tag{1}$$

$$\text{s.t } \|\mathbf{N}_{\mathrm{DUT}}(\boldsymbol{s} \circ \widehat{\boldsymbol{E}}_{\mathrm{DUT}}) - \widehat{\boldsymbol{E}}_{\mathrm{sc}}\|_2 \leq \kappa\sigma. \tag{2}$$

In the above, $\boldsymbol{s}$ are scattering amplitudes, $\widehat{\boldsymbol{E}}_{\mathrm{DUT}}$ is an estimate of the field incident on the DUT (computed from the source separation), $\widehat{\boldsymbol{E}}_{\mathrm{sc}}$ is the scattered field obtained from the source separation step, $\kappa \leq 1$ is a user-defined parameter and σ is the L_2-norm of the residual given by a phase-conjugation solution. The bound in (2) thus produces solutions with smaller residuals in L_2 than obtained by phase conjugation, with $\kappa < 1$ enabling even tighter bounds. The implementation uses the SPGL1 solver for MATLAB [24], [27]. While the general method is the same as presented in earlier work, the singly curved shape of the DUT required changes in certain parts. Since the previous work used planar geometries, care was taken to adapt the DUT mesh to be conformal to an arbitrary singly curved surface. Due to the large electrical size of the imaging problem, the operator $\mathbf{N}_{\mathrm{DUT}}$ in Fig. 1 is accelerated by exploiting translational invariance in the Green's function. For a planar DUT, translational invariance can be obtained in both x and y, making the operator similar to a Toeplitz matrix. Matrix-vector multiplications for this matrix type can be computed by fast Fourier transforms (FFT) [28], enabling the operator to be applied using a two-dimensional FFT. For the DUT geometry used in this work, translational invariance can only be obtained in y, changing the structure of the operator. The acceleration method was modified to reflect this, with the operator being applied using a combination of FFT's and summation instead.

As an alternative to the sparse imaging method, data is also processed using a Fourier method. A time reversal approach [14], [15] is used since this allows for imaging using single frequency data in two spatial dimensions. Since the method translates the signal from the measurement plane to other parallel planes, multiple translations are required for imaging on a singly curved surface. For each x-coordinate in the measured data, the signal is translated in $-z$ such that the resulting image plane intersects with the DUT surface at that x-coordinate. The image data along that intersection is then extracted, generating an image conformal to the DUT surface

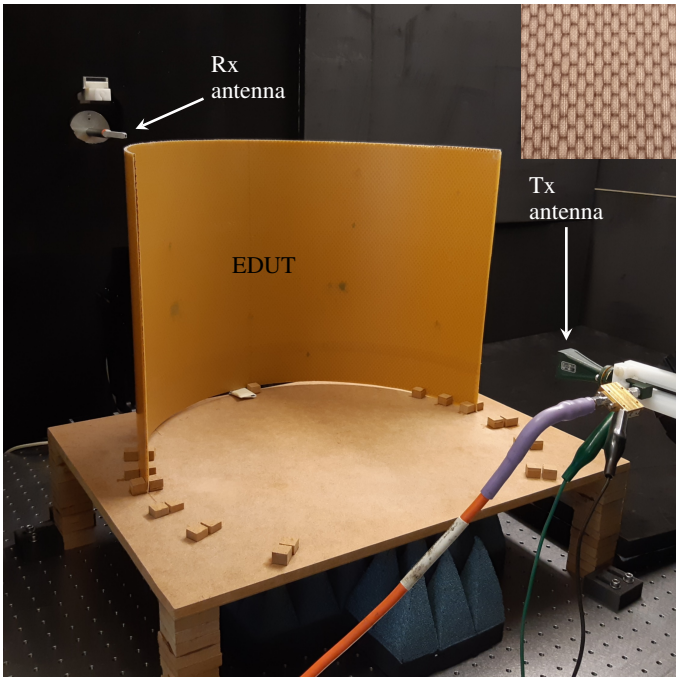

Fig. 2. Experimental setup with the example DUT (EDUT) mounted for imaging of its center. Top right inset shows close-up view of EDUT structure.

when this is done for every x. Finally, the image is normalized to that obtained from a reference measurement with the DUT absent.

III. Measurement Setup

Measurements were performed in the microwave laboratory at Lund University, Sweden. A photograph of the measurement setup is shown in Fig. 2, which can be compared to the schematic view in Fig. 1. The setup was mounted on a Newport RS 2000 optical table. The Tx antenna was a Flann 25240-20 standard gain horn and the Rx antenna was an MVG OEW5000 open-ended waveguide. An SHF 827 RF amplifier was used at the Tx end of the system to boost the signal level. The Rx antenna was scanned along the measurement surface using two THORLABS LTS300/M positioners. The Tx and Rx ends of the system were connected to a Rhode & Schwarz ZVA 67 GHz vector network analyzer (VNA) where S21 was measured. Measurements were performed for 201 linearly spaced frequency points in the band 55-65 GHz to allow for reduction of multipath propagation by time gating. The frequency of interest to image reconstruction was centered in this band at 60 GHz. A laptop was used to control measurements using a GPIB connection to the VNA and USB connections to the positioners. Data was then retrieved for all frequency points in 81×81 regularly spaced points over a 300 mm $\times$ 300 mm measurement plane, a scan which took roughly 7 h to complete. The sampling distance was thus 3.75 mm, which corresponds to $3\lambda/4$ at 60 GHz. This is in violation of the Nyquist criterion, which is of interest to Fourier based steps in the post-processing. However, the wavenumber spectrum at the Rx antenna is restricted by the beamwidth of the Tx antenna and the system geometry. This allows for a larger sampling distance before aliasing occurs than that given by the standard Nyquist criterion [29]. The DUT, referred to as the example DUT (EDUT) in the following, was an industrially manufactured composite panel provided by SAAB Aeronautics. The panel was shaped as a semi-circular cylindrical shell with a radius of 24 cm and a height of 35 cm. It was constructed as a sandwich-structured composite with a 2 mm low-permittivity overexpanded Nomex honeycomb core between two 0.5 mm sheets of Toray EX-1515, a cyanate ester quartz fabric pre-preg [30]. The adhesive Toray EX-1516, developed for bonding solid, honeycomb, or foam core structures used in aircraft and space applications [30], was used to assemble the panel and it was covered with a fluoropolymer film. A close-up of the EDUT showing the honeycomb structure is shown in the inset of Fig. 2.

A medium-density fiberboard platform was used to elevate the EDUT to a height appropriate for scanning of the Rx antenna. Blocks mounted on the top of the platform allowed for consistent rotation of the EDUT so that different parts could be imaged. The boresight distance between the Tx antenna and the EDUT was 570 mm, while the Rx antenna was scanned in a measurement plane 60 mm further away. These distances were selected to place the EDUT in the far-field of the Tx antenna, enable enough illumination of the EDUT and capture most of the scattered field in the measurement plane.

Two types of scans were performed: reference measurements and EDUT measurements. For the reference measurement, the setup was identical to that described above but with the EDUT removed. While one of the stated advantages of the sparse imaging approach was reference-free imaging, time reversal imaging required a reference measurement for normalization. EDUT measurements were performed with the EDUT rotated between scans, assisted by blocks mounted on the top of the platform. There was no overlap between imaged parts of the EDUT. The labels *right* and *left* used in following parts of this work refer to the directions when the EDUT is viewed from the Rx antenna towards the Tx antenna.

After capturing the data and before performing imaging, two post-processing steps were conducted: time gating and probe correction. As described earlier, a wideband measured signal was used for the purpose of reducing multipath components using time gating. More specifically, the frequency domain data for each spatial sample was zero-padded and transformed to the time domain where a Tukey window centered on the first peak in the signal was applied. A window length of 0.9 ns, corresponding to a 27 cm propagation distance in free space, was selected after inspection of the signal characteristics in the time domain. Transformation back to the frequency domain then resulted in a reduction of the multipath components of the signal. A single-frequency dataset at 60 GHz was extracted and probe correction was applied to it. This standard technique for open-ended waveguides, which is described in [8], [31], aims to remove the influence of the probe from measurement data. After these two post-processing steps, electric field data without multipath components could be obtained.

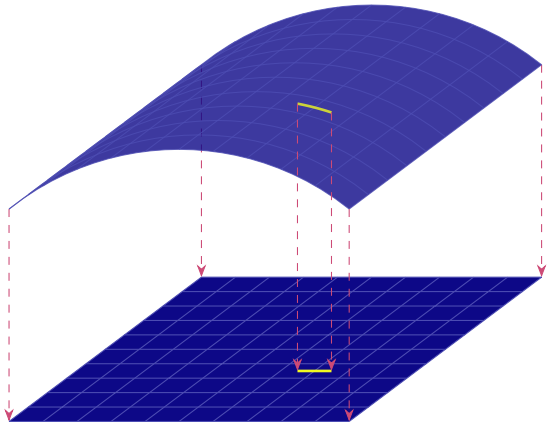

Fig. 3. Image on the singly curved EDUT surface together with the same image projected to an xy-plane.

IV. Imaging Results and Discussion

Images were generated from the time-gated and probe corrected measurement data using sparse imaging and time reversal imaging. To improve the resolution of the sparse images, a sub-sampling of 4 was used, replacing each mesh element on the EDUT by 4×4 smaller elements. The resolution of the time reversal images was equal to the measurement resolution as this was limited by the method itself. All processing was performed on a desktop computer with 32 GB RAM. While there were no processing parameters to set for time-reversal imaging, the sparse scatterer reconstruction step required selection of the parameters τ_{SVD} (truncation threshold in the SVD used in the source separation) and κ (from (2)) as discussed in [26]. For the images shown in this work, the parameters $\tau_{\mathrm{SVD}} = 0.01$ and $\kappa = 0.85$ were used.

In all images, reconstruction was done on the singly curved surface of the EDUT, but for visualization clarity they are shown here as planar images. These are projections from the original image on the singly curved surface to an xy-plane as illustrated in Fig. 3. The final images of the EDUT generated using time reversal imaging and sparse imaging are shown in Figs. 4 and 5 together with photos of the imaged parts of the EDUT. The color scale is equal for all images, although the quantities represented by that scale are different. This is done to illustrate differences in dynamic range between images rather than details in individual images.

Starting with the right part of the EDUT shown in Fig. 4, the sparse image in (b) shows six clearly visible indications which correspond to visual indications of flaws in (a). Most of the background is zero due to suppression of nonzero pixels by the L_1-minimization routine. For time reversal imaging in Fig. 4(c), it is seen that the indications are not as clearly distinguishable from the background as for sparse imaging. The resolution is also visibly lower as no sub-sampling could be performed. Of the visible indications, only the one near $(x, y) = (-30, 20)$ mm is similar to Fig. 4(b) in separation from the background. For other indications, the separation is only a few dB, which is not very far from the variation in the background. Those near $x = 100$ mm are especially difficult to distinguish due to the spurious background near the edges. The spurious background near the edges can be related to the normalization. Both the measured and reference fields have smaller main lobes after the time reversal translation, resulting in very low and noisy values near the edges. Normalization increases the low amplitudes, but the noise remains. Even away from the spurious values near the edges of the image, the background is not as homogeneous as in the sparse imaging case.

The left part of the EDUT is shown in Fig. 5. In this case, the sparse image in Fig. 5(b) shows four clear indications which correspond to visual indications in (a), and one weak indication near $(x, y) = (-100, 100)$ mm. In the background some clutter at low levels is visible. This can be attributed to the selected κ since a higher value would reduce clutter, but at the expense of the number of visible indications. For time reversal imaging in Fig. 5(c), the indications which were clear in (b) are seen but with the expected lower resolution and a smaller separation to the background. In the top left, it is difficult to identify a flaw due to the spurious background. There is one strong visual indication in the lower right of Fig. 5(a) which is not present in either (b) or (c). An additional transmission measurement was set up to investigate this discrepancy. This measurement was simpler than that used for the main results and consisted of the same Tx antenna in line with a fixed Rx probe connected to a ZVA67 VNA measuring S21 at 60 GHz. Different parts of the EDUT were moved between the antenna and the probe while S21 was monitored. All flaws affected S21 except for the one not seen in Figs. 5(b) and (c). Since three different methods using two separate measurements failed to detect that flaw, it is concluded that its electromagnetic properties are similar to the EDUT background medium. This apparent absence of electromagnetic contrast makes the detection failure less concerning as the purpose of our method is primarily to evaluate electromagnetic performance.

For both time reversal imaging and sparse imaging, it can be observed that some flaws near the edges of the measurement plane give weaker indications on images than those in the center, e.g. near $x = 100$ mm in Fig. 4(b). For time reversal imaging, this can be partly attributed to the spurious background near the edges. However, scattering amplitudes from sparse imaging are also weaker near the edges without any spurious background. One explanation for this effect lies in the collection of the scattered field. If the location of a scatterer is near the center of the measurement plane, a large part of the scattered field is captured by the measurement. For scatterers further away from the center, less of the scattered field is captured which gives less data for image reconstruction. A system implication of this is that the measurement plane should be larger than the section of interest on the DUT.

V. Conclusion

The aim of this work was to demonstrate a mm-wave imaging method developed for NDT of singly curved composite panels. A comparison has been made between our sparse imaging method and a more traditional time reversal imaging method. The sparse imaging method has been demonstrated to

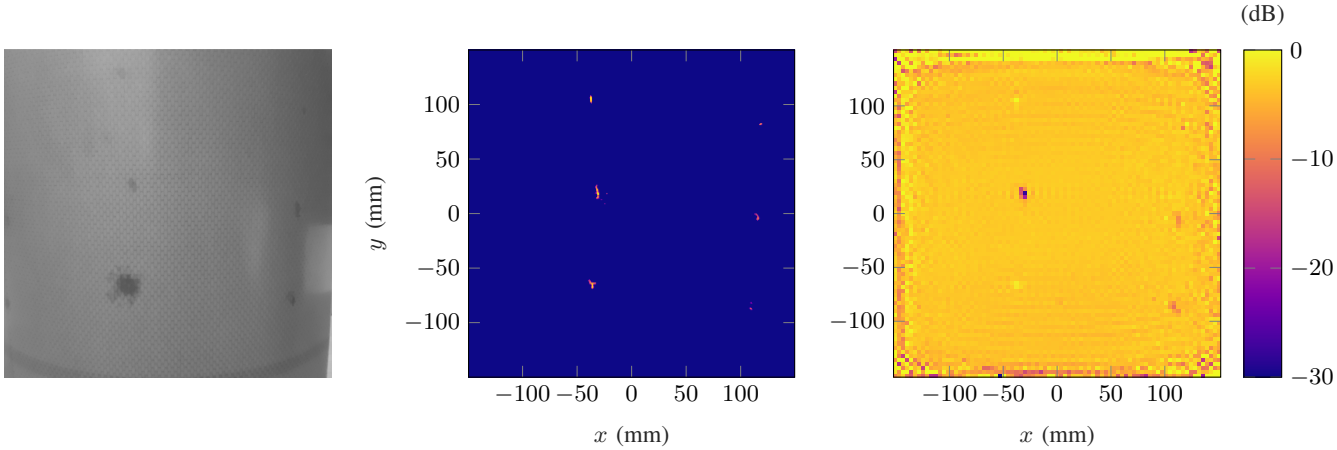

Fig. 4. Images for the right part of the EDUT retrieved using different methods. (a) Photo of the measurement area. (b) Absolute values of the scattering amplitudes from sparse imaging. (c) Amplitude of the time reversed field normalized to reference field.

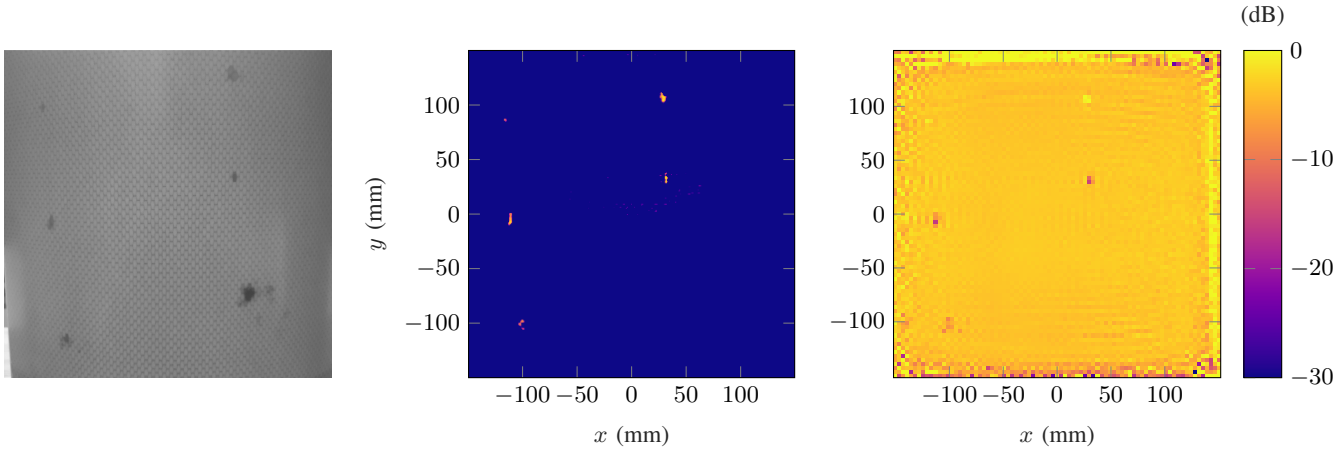

Fig. 5. Images for the left part of the EDUT retrieved using different methods. (a) Photo of the measurement area. (b) Absolute values of the scattering amplitudes from sparse imaging. (c) Amplitude of the time reversed field normalized to reference field.

provide images with multiple benefits over the time reversal imaging method such as higher resolution, higher dynamic range and more homogeneous background. While the method used in this work is an extension of one developed for planar DUTs, the imaging on singly curved DUTs presented in this work is likely to be more relevant to NDT on structures found in aerospace applications.

While the method presented in this work can be used for NDT of industrially manufactured panels as demonstrated, it can be improved upon to streamline usage in an industrial setting. One easily identified limitation is the measurement time, which was 7 h in this work. It could be reduced greatly by replacing the single Rx antenna used in this work with an antenna array. This comes at a cost and complexity deemed unnecessary at this stage, but would likely not impact the presented algorithms. Another limitation is the need to accurately know the DUT shape and position beforehand. In this work, a simple semi-circular cylindrical shell was used and it was carefully positioned. While more complicated DUTs can still have known geometries, the method could be made more versatile by the use of some other technology like 3D laser scanning for geometry characterization. This could also increase accuracy since small changes in DUT geometry and position can be accounted for. An interesting extension of this work would be to move from transmission-based to reflection-based imaging since NDT could then be performed with access to only one side of the DUT. While this extension was done for planar DUTs in our previous work, a more considerable effort would be needed to do the same for singly curved DUTs.

Acknowledgment

The authors would like to thank P. Hallander and M. Petersson at SAAB Aeronautics, Linköping, Sweden for manufacturing the composite panel. They would also like to thank C. Cederberg at the Department of Electrical and Information Technology, Lund University, for manufacturing mechanical components used in the measurements.

REFERENCES

[1] K. K. Chawla, *Composite Materials: Science and Engineering*, 4th ed. Cham, Switzerland: Springer International Publishing, 2019.

[2] P. Irving and C. Soutis, Eds., *Polymer Composites in the Aerospace Industry*, 2nd ed. Duxford, United Kingdom: Woodhead Publishing, 2020.

[3] M. Hagnell and M. Åkermo, "A composite cost model for the aeronautical industry: Methodology and case study," *Composites Part B: Engineering*, vol. 79, pp. 254 – 261, 2015.

[4] P. J. Shull, *Nondestructive evaluation: theory, techniques, and applications*. Boca Raton, FL, USA: CRC press, 2002.

[5] S. Kharkovsky and R. Zoughi, "Microwave and millimeter wave nondestructive testing and evaluation - overview and recent advances," *IEEE Instrumentation Measurement Magazine*, vol. 10, no. 2, pp. 26–38, April 2007.

[6] M. A. Abou–Khousa, A. Ryley, S. Kharkovsky, R. Zoughi, D. Daniels, N. Kreitinger, and G. Steffes, "Comparison of x-ray, millimeter wave, shearography and through-transmission ultrasonic methods for inspection of honeycomb composites," *AIP Conference Proceedings*, vol. 894, no. 1, pp. 999–1006, 2007.

[7] S. S. Ahmed, A. Schiessl, F. Gumbmann, M. Tiebout, S. Methfessel, and L. Schmidt, "Advanced microwave imaging," *IEEE Microwave Magazine*, vol. 13, no. 6, pp. 26–43, Sep. 2012.

[8] A. Yaghjian, "An overview of near-field antenna measurements," *IEEE Transactions on Antennas and Propagation*, vol. 34, no. 1, pp. 30–45, 1986.

[9] J. T. Case, M. T. Ghasr, and R. Zoughi, "Optimum two-dimensional uniform spatial sampling for microwave SAR-based NDE imaging systems," *IEEE Transactions on Instrumentation and Measurement*, vol. 60, no. 12, pp. 3806–3815, Dec 2011.

[10] M. J. Horst, M. T. Ghasr, and R. Zoughi, "A compact microwave camera based on chaotic excitation synthetic-aperture radar," *IEEE Transactions on Antennas and Propagation*, vol. 67, no. 6, pp. 4148–4161, June 2019.

[11] H. C. Rhim and O. Büyüköztürk, "Wideband microwave imaging of concrete for nondestructive testing," *Journal of Structural Engineering*, vol. 126, no. 12, pp. 1451–1457, 2000.

[12] T. Truong, A. Dinh, and K. Wahid, "An ultra-wideband frequency system for non-destructive root imaging," *Sensors*, vol. 18, no. 8, p. 2438, Jul 2018.

[13] M. A. Richards, J. A. Scheer, and W. A. Holm, Eds., *Principles Of Modern Radar*. Raleigh, NC, USA: SciTech Publishing, Inc., 2010, vol. 1: Basic Principles.

[14] R. H. Stolt, "Migration by Fourier transform," *Geophysics*, vol. 43, no. 1, pp. 23–48, 1978.

[15] C. Gilmore, I. Jeffrey, and J. LoVetri, "Derivation and comparison of SAR and frequency-wavenumber migration within a common inverse scalar wave problem formulation," *IEEE Transactions on Geoscience and Remote Sensing*, vol. 44, no. 6, pp. 1454–1461, 2006.

[16] D. Colton and R. Kress, *Inverse Acoustic and Electromagnetic Scattering Theory*, 3rd ed. Cham, Switzerland: Springer Nature Switzerland AG, 2019.

[17] P. C. Hansen, *Discrete Inverse Problems : Insight and Algorithms*. Philadelphia, PA, USA: Society for Industrial and Applied Mathematics, 2010.

[18] N. Joachimowicz, C. Pichot, and J. P. Hugonin, "Inverse scattering: an iterative numerical method for electromagnetic imaging," *IEEE Transactions on Antennas and Propagation*, vol. 39, no. 12, pp. 1742–1753, 1991.

[19] S. Caorsi, A. Massa, M. Pastorino, and M. Donelli, "Improved microwave imaging procedure for nondestructive evaluations of two-dimensional structures," *IEEE Transactions on Antennas and Propagation*, vol. 52, no. 6, pp. 1386–1397, 2004.

[20] K. Persson, M. Gustafsson, G. Kristensson, and B. Widenberg, "Radome diagnostics—source reconstruction of phase objects with an equivalent currents approach," *IEEE Transactions on Antennas and Propagation*, vol. 62, no. 4, pp. 2041–2051, 2014.

[21] T. F. Eibert and C. H. Schmidt, "Multilevel fast multipole accelerated inverse equivalent current method employing Rao–Wilton–Glisson discretization of electric and magnetic surface currents," *IEEE Transactions on Antennas and Propagation*, vol. 57, no. 4, pp. 1178–1185, April 2009.

[22] J. L. A. Quijano and G. Vecchi, "Field and source equivalence in source reconstruction on 3D surfaces," *Progress In Electromagnetics Research*, vol. 103, pp. 67–100, 2010.

[23] M. Zibulevsky and M. Elad, "L1-L2 optimization in signal and image processing," *IEEE Signal Processing Magazine*, vol. 27, no. 3, pp. 76–88, 2010.

[24] E. van den Berg and M. P. Friedlander, "Probing the Pareto frontier for basis pursuit solutions," *SIAM Journal on Scientific Computing*, vol. 31, no. 2, pp. 890–912, 2008.

[25] J. Helander, A. Ericsson, M. Gustafsson, T. Martin, D. Sjöberg, and C. Larsson, "Compressive sensing techniques for mm-wave nondestructive testing of composite panels," *IEEE Transactions on Antennas and Propagation*, vol. 65, no. 10, pp. 5523–5531, Oct. 2017.

[26] J. Helander, J. Lundgren, D. Sjöberg, C. Larsson, T. Martin, and M. Gustafsson, "Reflection-based source inversion for sparse imaging of low-loss composite panels," *IEEE Transactions on Antennas and Propagation*, vol. 68, no. 6, pp. 4860–4870, 2020.

[27] E. van den Berg and M. P. Friedlander, "SPGL1: A solver for large-scale sparse reconstruction," December 2019. [Online]. Available: https://friedlander.io/spgl1

[28] G. H. Golub and C. F. V. Loan, *Matrix Computations*, 3rd ed. Baltimore, MD, USA: Johns Hopkins University Press, 1996.

[29] A. C. Newell, "Error analysis techniques for planar near-field measurements," *IEEE Transactions on Antennas and Propagation*, vol. 36, no. 6, pp. 754–768, 1988.

[30] Toray Advanced Composites. Accessed Sept. 24, 2021. [Online]. Available: https://www.toraytac.com/

[31] A. Yaghjian, "Approximate formulas for the far field and gain of open-ended rectangular waveguide," *IEEE Transactions on Antennas and Propagation*, vol. 32, no. 4, pp. 378–384, 1984.